

Fluctuation of the phase boundary in the six-vertex model with Domain Wall Boundary Conditions: a Monte Carlo study

Ivar Lyberg^{*1}, Vladimir Korepin², and Jacopo Viti^{†3}

¹ PhD Stony Brook University

²C.N. Yang Institute for Theoretical Physics, Stony Brook University, Stony Brook, New York, 11794-3840, USA

³Dipartimento di Fisica, Università di Firenze, via G. Sansone 1, 50019 Sesto Fiorentino, Italy

Abstract

We consider the six-vertex model with Domain Wall Boundary Conditions. Our main interest is the study of the fluctuations of the extremal lattice path about the arctic curves. We address the problem through Monte Carlo simulations. At $\Delta = 0$, the fluctuations of the extremal path along any line parallel to the square diagonal were rigorously proven to follow the Tracy-Widom distribution. We provide strong numerical evidence that this is true also for other values of the anisotropy parameter Δ ($0 \leq \Delta < 1$). We argue that the typical width of the fluctuations of the extremal path about the arctic curves scales as $N^{1/3}$ and provide a numerical estimate for the parameters of the scaling random variable.

1 Introduction

In probability theory [1], the sum of a large number of random variables might approach a deterministic value. For instance, the law of large numbers implies that the sample mean of N independent identically distributed random variables converges to their distribution average for large N . Moreover, if those random variables have finite variance, fluctuations of their sum are normally distributed with a variance of order \sqrt{N} . The convergence toward smooth functions of combinations of a large number of random variables is at the root of the effectiveness of the methods of statistical mechanics and also provides a solid ground for numerical techniques such as Monte Carlo. This phenomenon is not restricted to local observables but extends to geometrical quantities such as random curves. An instructive example discussed in [2] but see also [3] is a one-dimensional random walk starting from the origin and conditioned in T steps to reach the point X . For large X and T with $X/T = v$ finite, the random paths performed by the walker are with probability one within any neighborhood of the classical trajectory $X = vT$. Limit shapes [4] are smooth nonrandom curves that describe the thermodynamic limit of random lattice paths. Historically, one of the most studied examples is the arctic circle [5] that appears in dimer coverings of the Aztec diamond. This domino tiling problem is equivalent [6] to the

^{*}ivar.lyberg@hotmail.com

[†]jacopo.viti1@unifi.it (corresponding author)

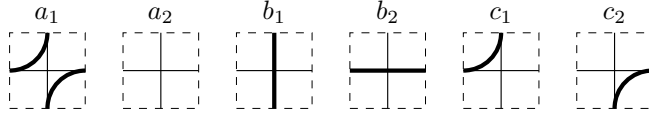


Figure 1: The six possible configurations of a lattice path in the six-vertex model are denoted by thick lines. The continuous lines are lattice edges while dashed lines are edges of the dual lattice.

six vertex model [7, 8] with Domain Wall Boundary Conditions (DWBC) at its free fermionic point [9, 10, 11].

Let N be a positive integer, a configuration of the six vertex model on a $N \times N$ square lattice with DWBC [12, 13, 14, 15, 16, 17] is specified by N non-intersecting paths traveling on the edges of the lattice. On each vertex, the path can have the six possible configurations given in Fig. 1; the Boltzmann weights associated with those are a for the vertices of type a_1 and a_2 , b for the vertices of type b_1 and b_2 and c for the vertices of type c_1 and c_2 . To characterize the phase diagram of the model, it is useful to introduce the parameter Δ [9], defined as

$$\Delta := \frac{a^2 + b^2 - c^2}{2ab}.$$

In this work, we will focus on the domain $0 \leq \Delta < 1$, which is included in the so-called disordered phase $|\Delta| < 1$ see [18] for a comprehensive study of the phase diagram. The case $\Delta = 0$ is the free fermionic point mentioned a few lines above.

The N random paths enter the lattice from above and exit from the left, see Fig. 2 on the left. Since they cannot intersect, for large enough N they can fluctuate only within a region whose boundary is arbitrarily close to a curve, dubbed the arctic curve [5]. For $\Delta = 0$ and $a = b$, such a curve is the circle $(x/R)^2 + (y/R)^2 = 1$, depicted in Fig. 2 and inscribed in the square lattice. Inside the arctic curve the model is in a disordered phase, outside is in a trivial ferromagnetic phase. The Cartesian coordinates are also defined in Fig. 2 and lengths, such as the circle radius R , are measured in suitable lattice units. In this paper, we follow the convention to divide the square diagonal into N intervals, therefore x, y are semi-integers in the interval $[-N/2, N/2]$; for simplicity, we assume N a power of two from now on.

The Cartesian equation of the arctic curve depends on the parameter Δ and was calculated in [19, 20], see also [3]. The limit shape, however, is a property of the model in the thermodynamic limit and it is relevant to understand how the interface between the disorder and the ferromagnetic phase fluctuates due to finite-size effects. In this case, the phases are not separated by a smooth curve; rather, the distance from a corner to the disordered phase varies according to a probability distribution. Consider, for instance, a quarter of the original lattice: the southeast (SE) quadrant on the right of Fig. 2. When N is large, there are no paths in a neighborhood of the SE corner and all the vertices are of type a_2 . For later purposes, introduce the parameter η as

$$\eta := 2y/N. \quad (1)$$

Take $|\eta| < 1/2$; as we move along a constant- y line toward the boundary, we cross $N/4$ lattice paths, see Fig. 2. Denote then by $X_{ext}(\eta)$ the x -coordinate of the intersection of a constant- y line with the furthest path from the origin. Refs. [21, 22] tackled rigorously the study of the fluctuations of the extremal path in the context of dimer coverings. The same conclusions apply to the six-vertex with DWBC at $\Delta = 0$, [6]. In particular, it can be proven that for $N \gg 1$, the scaling random variable

$$\mathcal{Z}_0(\eta) := \pm \frac{X_{ext}(\eta) - \Lambda(\eta)N}{\Gamma(\eta)N^{1/3}} \quad (2)$$

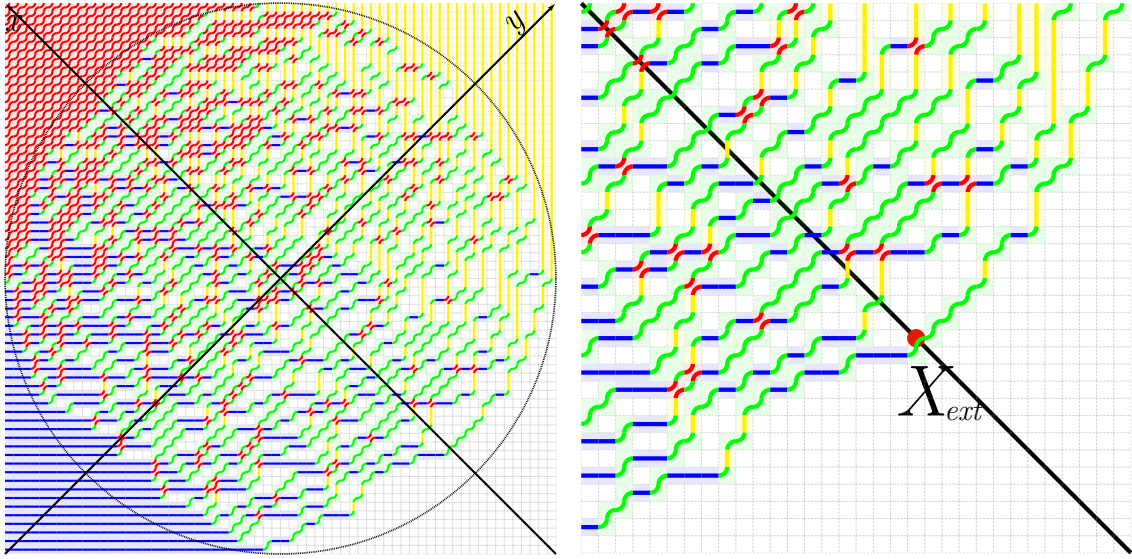


Figure 2: **Left.** Lattice path configuration in the six vertex model with DWBC for $N = 64$, and $a = b$ at $\Delta = 0$. The possible vertex configurations have been colored differently: vertices of type a_1 are colored in red, of type a_2 in white, of type b_1 in yellow, of type b_2 in blue while of type c_1 and c_2 in green. The black circle is the arctic curve for the given choice of the parameters. **Right.** The SE corner of the lattice path configuration on the left for $N = 64$. The furthest path from the center of the lattice intersects a constant y line in a point with abscissa $X_{ext}(\eta)$. The picture shows $X_{ext}(\eta = 0)$.

obeys a Tracy-Widom (TW) distribution [23] for any $|\eta| < 1/2$. The sign in front of Eq. (2), is the one of $X_{ext}(\eta)$ in the coordinate system defined in Fig. 2. Moreover, the parameters Λ and Γ are $O(1)$: ΛN is the x -coordinate of the intersection of the arctic curve (an ellipse if $a \neq b$) with the constant- y line while Γ can be derived from Ref. [24], see Sec. 3.

The TW distribution characterizes fluctuations of extrema of random variables in several different contexts, among them: the spectrum of Hermitian random matrices [23], ordered sequences in random permutations [25], random growth models [21, 26] and their generalizations [27, 28], the KPZ equation [29], quantum dynamics [30, 24, 31]. Many of these problems can be mapped into each other [32] and one might wonder [33] how universal is the TW distribution.

In this paper, we will study numerically the probability distribution of $X_{ext}(\eta)$ for values of $\Delta \neq 0$ in the interval $[0, 1)$. We will argue that after a rescaling analogous to Eq. (2), this random variable follows, for large enough N , again a TW distribution. The main outcome of our study is summarized in Fig. 6. This result is not unexpected and can be justified heuristically. Non-intersecting lattice paths can be mapped to fermionic trajectories in a Euclidean space time. The fermionic particles are interacting if $\Delta \neq 0$, however the particle furthest from the origin, which is also the fastest, behaves as if were free [32, 34, 35]. This observation is also at the root of the so-called tangent method [3].

The rest of the paper is organized as follows. In Sec 2, we review briefly the numerical method. In Section 3 we discuss the comparison with the case $\Delta = 0$ and further analyze the lattice path fluctuations for $\Delta \neq 0$ in Sec. 4. Finally, in Sec. 5 we summarize our conclusions.

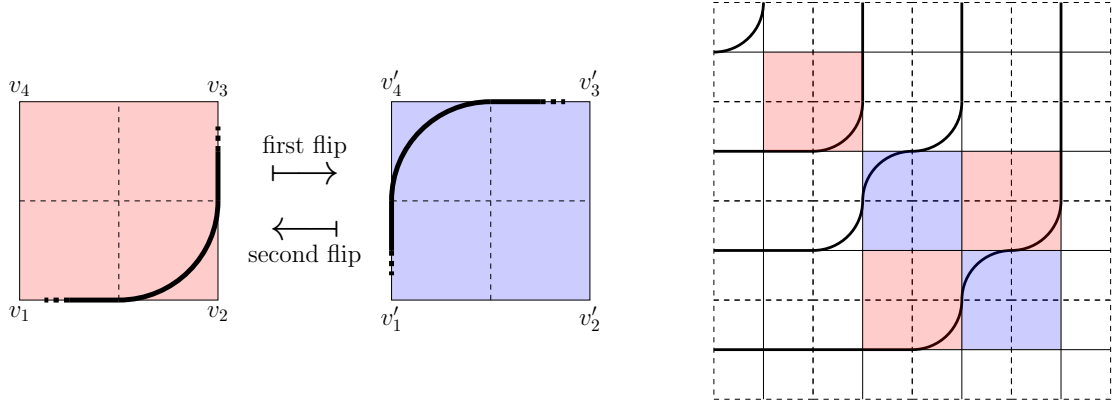


Figure 3: **Left.** The two MC moves. **Right.** The six-vertex model with DWBC with $N = 4$. The picture also shows an allowed state. This state has four flippable plaquettes. The plaquettes indicated in blue, are second flippable while the plaquettes indicated in red are first flippable.

2 Monte Carlo study of the six-vertex model with DWBC

Method.—We modify a Monte Carlo (MC) algorithm for simulating the six-vertex model with DWBC that was originally proposed in [36]. The MC algorithm involves two moves called first flip and second flip; see Fig. 3. The moves may modify the configuration of the paths along the edges of a plaquette of the square lattice. The state S of a plaquette is a list that contains the configurations of its four vertices: $S = \{v_1, v_2, v_3, v_4\}$, with v_i given in Fig. 1. The Boltzmann weight of v_i will be denoted by $w(v_i) = a, b, c$. The weight of the state S is then $W(S) = \prod_{i=1}^4 w(v_i)$. An MC move takes then a state S to a new state S' . Since in a flippable plaquette, each vertex can have two possible configurations, there are sixteen distinct plaquette states which are respectively first or second flippable. They have up to nine distinct weights.

The computer code has two lists, each containing the plaquettes flippable in one of the two different ways. We can formulate the algorithm as follows. First, randomly search among all plaquettes on the lattice, until a plaquette contained in one of the two lists is found. A flip will then be attempted, and if the attempt is successful, then both lists will be updated: at the plaquette itself and at the four plaquettes sharing a side with it. The probability P of an attempted flip that modifies the state of the plaquette S into S' is the Boltzmann weight of the new state, namely

$$P = W(S'). \quad (3)$$

In the computer program, the largest of the three weights a, b , and c is 1 and therefore Eq. (3) is well defined. The above conditions satisfy detailed balance and ensure ergodicity. An equivalent MC algorithm with Glauber dynamics has been employed in [37] and [38] to obtain numerical estimates for the arctic curves and one-point functions of the model with several values of Δ in the disorder phase. To ensure the system has thermalized we rely then on the results of those papers. We define a MC sweep as N^2 accepted flips. The largest value of N used in this paper is 256 whereas the longest side of the lattice used in the mentioned papers was as long as 500 units. We, therefore, consider it known at this time how long this system needs to equilibrate. From a rigorous perspective, Ref. [39] shows that the Glauber dynamics is rapidly mixing at $\Delta = 1/2$, while Refs. [40, 41] proved that the Markov chain exponentially slows down for large and negative Δ .¹ A reliable test of the TW distribution is challenging in a statistical model, see

¹The arguments of [41] break down in the whole disorder phase and although not rigorously proven, it is expected that Glauber dynamics is rapidly mixing for all $|\Delta| < 1$.

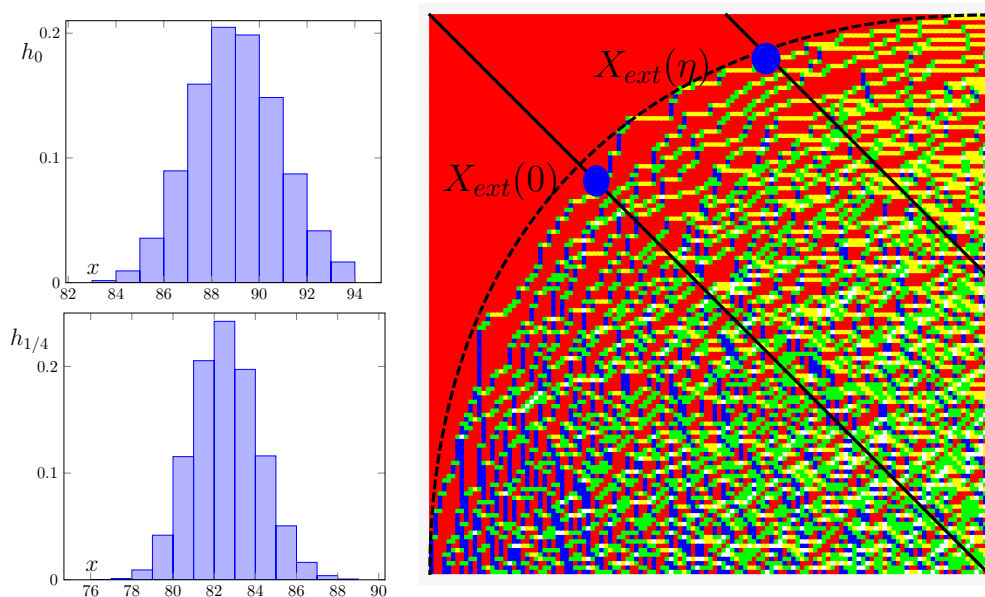


Figure 4: **Left.** We show the numerical data for distributions of the random variables $X_{ext}(\eta = 0)$ and $X_{ext}(\eta = 1/4)$ along the lines $y = 0$ and $y = N/8$, see also Eq. (1), at $\Delta = 1/2$ and $N = 256$. **Right.** A realization of the random variable $X_{ext}(\eta)$ for two different values of η at $\Delta = 1/2$ and $N = 256$.

for instance [42] and requires a much larger number of sweeps than that employed previously in Refs. [37, 38]. In this paper, we will construct samples with 10^6 MC sweeps.

In the disorder phase, analogous MC algorithms are nowadays commonly adopted in numerical experiments with the six vertex model [43, 44, 45, 46, 47, 48]. For earlier numerical approaches to ice models, see [49, 50]. Finally, an efficient algorithm to simulate interacting dimers has been proposed in [51] but so far it has not been implemented in the six-vertex model. *The extremal lattice path.*—In the coordinate system² defined in Fig. 1 with origin in the center of the lattice, the random variable $X_{ext}(\eta)$ is the position, along a line at constant y , of the last occurrence of a vertex of different type from those around the frozen corner. The right panel of Fig. 4 illustrates a realization of $X_{ext}(\eta)$ for $\eta = 0$ and $\eta = 1/4$ on the NW corner of lattice with $N = 256$ and $\Delta = 1/2$. Nearby this corner the vertices are in the state a_1 , see Fig. 1 and Fig. 2; the black dashed line is the arctic curve [19].

The probability distribution, $\text{Prob}(X_{ext}(\eta) = x)$, will be approximated numerically at finite N by a normalized histogram which we denote by h_η ; see Sec. 4.2 for more detail about its construction. The left panel of Fig. 4 shows two examples at $\eta = 0$ and $\eta = 1/4$ for $\Delta = 1/2$ and $N = 256$. The two histograms are not symmetric (the right tail is longer than the left) and obviously have different variance and mean. Their properties will be studied in the next two sections.

²Notice that in Ref. [24], the square diagonal is divided into $2N$ intervals. Therefore distances measured along the diagonal in this paper are twice as big as the ones considered in [24]. This choice also implies that the constant Γ in Eq. (2) is half of the one obtained analytically in [24] at $\Delta = 0$, see Sec. 3.

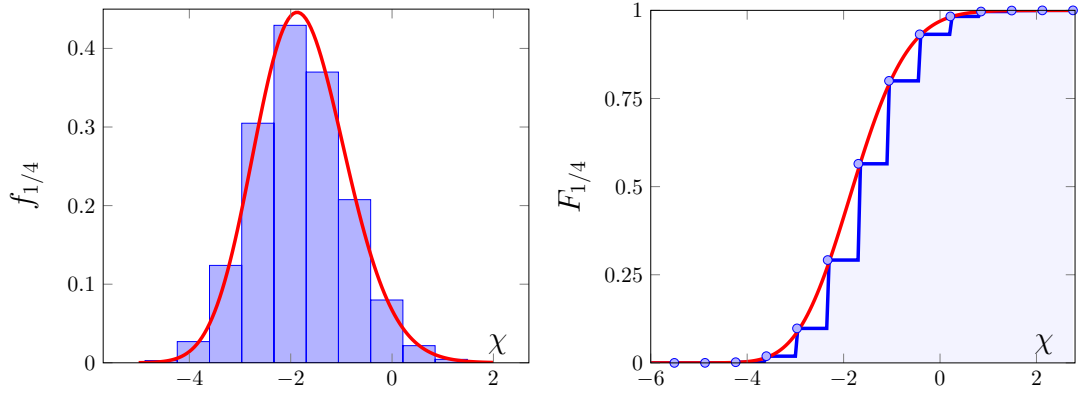


Figure 5: **Left.** Distribution of the random variable $\mathcal{Z}_0(\eta)$ defined in Eq. (2) calculated from the MC simulation at $\eta = 1/4$ and $N = 256$ for $\Delta = 0$. The red curve is the TW distribution $\mathcal{F}'_2(\chi)$. There are no free parameters in the comparison. **Right.** The empirical cumulative distribution of the random variable $\mathcal{Z}_0(\eta)$ is plotted together with the cumulative distribution \mathcal{F}_2 at $\eta = 1/4$ and $N = 256$ for $\Delta = 0$.

3 Results at $\Delta = 0$

Special attention must be paid to the case $\Delta = 0$, since it is the only point at which there are known exact results for the random process that describes the fluctuations of the coordinate $X_{ext}(\eta)$. Let us take for simplicity $a = b$; in [22, 21], the random fluctuations were proven for large N to converge to the so-called Airy process for any $|\eta| < 1/2$. By following [24], we can derive analytically the parameters Γ and Λ in Eq. (2). It turns out that

$$\Lambda(\eta) = \pm \frac{1}{2} \sqrt{\frac{1}{2} - \eta^2} \quad (4)$$

$$[\Gamma(\eta)]^3 = \frac{(1 - 4\eta^2)^2}{16(2 - 4\eta^2)^{3/2}}, \quad (5)$$

where the two branches of Eq. (4) depend on the sign of $X_{ext}(\eta)$. Notice that $\Gamma(\eta)$ is positive and monotonically decreasing with $\Gamma(1/2) = 0$. When the right-hand-side of Eq. (5) vanishes, the intersection point $X_{ext}(1/2) = N/4$ lies on the boundary of the square-lattice and its fluctuations are no longer described by the TW distribution. In this case, Ref.[52], see also [53] for a related discussion, proved that the latter are Gaussian with an horizontal width $O(\sqrt{N})$.

We then exploit Eqs. (4) and (5) to benchmark the validity of the MC simulation. In particular, according to Eq. (2), the probability distribution ($\text{Prob}(\mathcal{Z}_0(\eta) = \chi)$) of the random variable \mathcal{Z}_0 can be evaluated numerically as ³

$$f_\eta(\chi) = \Gamma(\eta) N^{1/3} h_\eta(\lfloor \Gamma(\eta) N^{1/3} \chi + N \Lambda(\eta) \rfloor). \quad (6)$$

Upon substituting Eqs. (4) and (5) into Eq. (6), one compares the MC data at finite N with the TW distribution $\mathcal{F}'_2(\chi)$. The result of this comparison is displayed on the left of Fig. 5 for $\eta = 1/4$ and $N = 256$. It shows a convincing agreement already for such a value of the lattice size; it should be remarked that there are no free parameters.

From a statistical viewpoint, it is possible to verify if the random variable \mathcal{Z}_0 is distributed according to \mathcal{F}'_2 , by performing a Kolmogorov-Smirnov test [54]. The latter requires to construct the empirical cumulative distribution of \mathcal{Z}_0 , which will be denoted by $F_\eta(\chi)$. On the

³The notation $\lfloor x \rfloor$ indicates the integer part of x .

N	$\Delta = 0$	$\Delta = 3/8$	$\Delta = 1/2$	$\Delta = 5/8$
64	1.822(13)	2.465(12)	2.849(14)	3.47(3)
128	3.348(12)	4.557(22)	5.32(4)	6.47(3)
256	6.29(7)	8.60(14)	10.05(16)	12.46(24)

Table 1: The parameter α_N as a function of N and Δ . The values of N are contained in the leftmost column and the values of Δ are shown in the uppermost row. The number in the bracket is the estimated error in the last digit.

right panel of Fig. 5 is plotted $F_\eta(\chi)$ at $\eta = 1/4$ and $N = 256$ together with the cumulative distribution of the TW distribution, denoted by $\mathcal{F}_2(\chi)$. The test statistics [55, 56] is $D_n := \sqrt{n} \sup_\chi |F_\eta(\chi) - \mathcal{F}_2(\chi)|$, where n is the number of points in Fig. 5. For $n = 14$, we obtain $D_{14} = 1.021 \dots$, which corresponds to a p -value of about 0.2 [57], well above the conventionally accepted threshold of 0.1.

We conclude therefore that the numerical results at $\Delta = 0$ are fully consistent with the available theoretical predictions and proceed to the cases $\Delta \neq 0$.

4 Results at $\Delta \neq 0$

For large N , when $\Delta = 0$, the distribution of the fluctuations of the random variable $X_{ext}(\eta)$ has the same functional form (see Eq. (6) and Eq. (2)) along any constant- y line as long as $|y| < N/4$. Such a distribution moreover depends on η in Eq. (1) only through its mean and variance.

We will now assume that, for large enough N , the same holds for all $0 \leq \Delta < 1$. In particular, after a linear η -dependent transformation, all the random variables $X_{ext}(\eta)$, will be also equally distributed. We can then maximize the amount of information available from a single sample by taking the average over all such probability distributions.⁴ The averaging procedure, described in detail in sec. 4.2, provides a better numerical approximation of the statistics of $X_{ext}(0)$ at $\Delta \neq 0$, see Fig. 6. In analogy with the case $\Delta = 0$ discussed in sec. 3, one constructs then the empirical probability distribution of the random variable,

$$\mathcal{Z}_\Delta(0) := \frac{X_{ext}(0) - \beta_N}{\alpha_N^{1/3}} \quad (7)$$

and compare it with the TW distribution by fitting the parameters α_N and β_N . It is expected that α_N is $O(N)$ for large N with a non-universal Δ -dependent proportionality constant. In sec. 4.2, we will present the main outcomes of the numerical analysis, its consistency with the analytic results at $\Delta = 0$ together with a numerical extrapolation of the non-universal coefficient.

4.1 Numerical evaluation of the distribution of \mathcal{Z}_Δ in Eq. (7)

For simplicity, we will consider only the isotropic case $a = b$. Consider the $1 + k_{\max}$ parallel lines $y = y_k$ with $y_k = k/2$ and $k = 0, 1, \dots, k_{\max}$, see Fig. 2, and define, see Eq. (1),

$$\eta_k := 2y_k/N = k/N. \quad (8)$$

⁴We calculate numerically the average of the distributions and not the distribution of the average; the two are of course very different. In particular, since the random variables $X_{ext}(\eta)$ are correlated, the latter does not follow the central limit theorem [1].

As discussed before, the parameter k_{\max} must be below $N/2$, in this paper we chose $k_{\max} = N/4$. We begin by describing how the distribution of the random variable X_{ext} , along the line $y = 0$, that is the lattice diagonal, will be constructed. We start with a random lattice state $S^{(0)}$ and an $N/2$ -dimensional vector $v_0^{(0)}$:

$$v_0^{(0)} = (0, 0, 0, \dots, 0). \quad (9)$$

The state $S^{(0)}$ will be used to obtain a new vector $v_0^{(1)}$ in the following way. We move from each of the four corners towards the center of the lattice until the first vertex with a state different from the state at the corner is met. The integer variable x will be used to count the steps. For example, beginning at the NW corner at $x = 0$, we walk along the diagonal until, at step $x = x_{NW}$, we reach a vertex which has a state different from a_1 . Beginning instead at the SW corner, we continue until we reach a vertex which does not have state b_2 ; and so on. The vector $v_0^{(1)}$ will then have the entries

$$v_0^{(1)}(x) = v_0^{(0)}(x) + \sum_{\iota \in \{\text{NE}, \text{NW}, \text{SW}, \text{SE}\}} \delta_{x, x_\iota}; \quad x = 0, 1, \dots, N/2 - 1. \quad (10)$$

Next, we perform one MC sweep, see Sec. 2. This will generate a new, independent random lattice state $S^{(1)}$. The process is then repeated and we will obtain a new vector $v_0^{(2)}$ from the vector $v_0^{(1)}$ and the state $S^{(1)}$. Altogether $T - 1$ sweeps will be made. The final vector $v_0^{(T-1)}$ will thus be obtained from T states $S^{(0)}, S^{(1)}, \dots, S^{(T-1)}$. It is convenient to use the opposite direction, from the center of the lattice towards the corner. To this end, we define the normalized histogram h_0 , see Sec. 4.2, as follows

$$h_0(x) := v_0^{(T-1)}(N/2 - 1 - x)/4T; \quad x = 0, 1, \dots, N/2 - 1. \quad (11)$$

The distribution obtained from Eq. (11) is illustrated on the upper left side of Fig. 4 for $\Delta = 1/2$ and $N = 256$. Here x is the distance from the center along the diagonal, which in the coordinate systems of Fig. 2 coincides indeed with the value of the x -coordinate in the NW corner. As mentioned in Sec. 1, the diagonal distance between two neighboring vertices is 1. In this paper, T will have the value $T = 10^6$ throughout.

We now would like to average over $1 + k_{\max}$ different distributions. First of all, the other k_{\max} vectors $\{v_{\eta_k}^{(T-1)}\}_{k=1}^{k_{\max}}$ are constructed in essentially the same way. The difference is that the process is begun on side of the lattice and not in the corner. Therefore, there are eight simultaneous processes and not four. We thus obtain another set of vectors $\{v_{\eta_k}^{(T-1)}\}_{k=1}^{k_{\max}}$. From these, we will obtain normalized, reversed histograms $\{h_{\eta_k}\}$ if, for each $k = 1, \dots, k_{\max}$, we define h_{η_k} as

$$h_{\eta_k}(x) := v_{\eta_k}^{(T-1)}(N/2 - 1 - x + y_k)/8T; \quad x = -y_k, \dots, N/2 - 1 - y_k. \quad (12)$$

The histogram $h_{1/4}(x)$ obtained when $k = k_{\max} = N/4$ is displayed for $\Delta = 1/2$ and $N = 256$ on the bottom left of Fig. 4.

We next calculate the mean μ_k and the variance σ_k of the distributions h_{μ_k} for all $k = 0, \dots, k_{\max}$. We have

$$\mu_k = \sum_{x=-y_k}^{N/2-1-y_k} x h_{\eta_k}(x), \quad \sigma_k^2 = \sum_{x=-y_k}^{N/2-1-y_k} (x - \mu_k)^2 h_{\eta_k}(x). \quad (13)$$

At this point, we will leave the actual lattice and define our distributions in a new, one-dimensional space. To perform with greater numerical accuracy the averaging procedure, it is convenient to

magnify the bin width by a constant factor θ , such that $1 < \theta < k_{\max}$. In terms of the new variable $t = \theta x$, the probability distributions in Eq. (12) are then ⁵

$$h_{\eta_k}^\#(t) = \frac{1}{\theta} h_{\eta_k} \left(\left\lfloor \frac{t}{\theta} \right\rfloor \right). \quad (14)$$

The value $\theta = 8$ will be used in this paper. By following the assumption stated at the beginning of this section, we further perform for all $k = 0, \dots, k_{\max}$ the linear change of variable

$$\xi = \frac{\sigma_0}{\sigma_k} (t - \theta \mu_k), \quad (15)$$

which transforms the probability distributions of Eq. (14) into

$$h_{\eta_k}^b(\xi) = \frac{\sigma_k}{\theta \sigma_0} h_{\eta_k} \left(\left\lfloor \frac{\sigma_k}{\sigma_0 \theta} \xi + \mu_k \right\rfloor \right). \quad (16)$$

It is easy to show, by recalling Eq. (13), that all the probability distributions in Eq. (16) have zero mean and variance $(\theta \sigma_0)^2$. According to our working hypothesis, they are then different histogram representations of the same probability distribution of the random variable

$$\Xi := \theta X_{ext}(\eta = 0) + C. \quad (17)$$

In Eq. (17), C is a constant that ensures that Ξ has zero mean. We estimate the probability distribution of the random variable Ξ with the average

$$\bar{h}_0(\xi) := \frac{1}{1 + k_{\max}} \sum_{k=0}^{k_{\max}} h_{\eta_k}^b(\xi); \quad (18)$$

in Eq. (18) the variable ξ belongs to the union of all the support of the histograms h_{η_k} in Eq. (16). In analogy with the case $\Delta = 0$ we test whether \mathcal{Z}_Δ in Eq. (7) obeys the TW distribution for large enough N and suitable parameters α_N and β_N . Recalling then Eq. (17), we numerically analyze whether

$$\bar{h}_0(\xi) \xrightarrow{N \gg 1} \frac{1}{\alpha_N^{1/3} \theta} \mathcal{F}_2' \left(\frac{\xi - \tilde{\beta}_N}{\alpha_N^{1/3} \theta} \right), \quad (19)$$

with \mathcal{F}_2' , the TW distribution and $\tilde{\beta}_N = C + \theta \beta_N$.

4.2 Analysis of the numerical results

Eq. (19) is equivalent to the statement that the probability distribution of \mathcal{Z}_Δ in Eq. (7) is

$$\bar{f}_0(\chi) = \alpha_N^{1/3} \theta \bar{h}_0(\alpha_N^{1/3} \theta \chi + \tilde{\beta}_N) \quad (20)$$

and the latter converges to the TW distribution for large N and any $0 \leq \Delta < 1$. On the left of Fig. 6, we show on the same plot the numerical results for $\bar{f}_0(\chi)$ at $N = 256$ and $\Delta = 0, \frac{3}{8}, \frac{1}{2}, \frac{5}{8}$. The continuous red curve underneath, which is barely visible, is the TW distribution $\mathcal{F}_2'(\chi)$. The agreement is already excellent at $N = 256$ and strongly supports the

⁵The entries of histograms are now indexed by $\theta k_{\max} + 1$ integers and, provided they have the same mean and variance, can be summed without the need of defining a piecewise function on the reals. The optimal value of θ is chosen in order to render the averaged histogram as smooth as possible. Its effect on the fluctuations of the random variable X_{ext} can be trivially traced back, see Eq. (19).

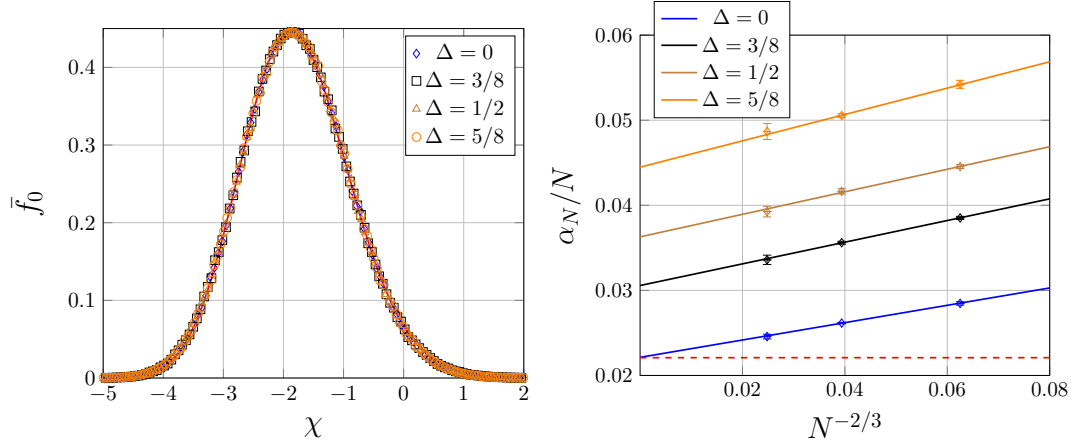


Figure 6: **Left.** Numerical data for the distribution $\bar{f}_0(\chi)$ in Eq. (20) at different values of Δ and $N = 256$. The parameters α_N and $\tilde{\beta}$ are obtained by requiring a best fit of the data with the TW distribution, which is the red curve underneath. **Right.** Numerical data for α_N/N from Tab. 1 together with the regression lines, see Eq. (21). The Pearson χ^2 is $O(1)$. The red dashed line is the analytical result for the y -intercept at $\Delta = 0$, obtained from Eq. (5) with $\eta = 0$.

universality hypothesis [32, 33] for the fluctuations of \mathcal{Z}_Δ in Eq. (7). The parameters α_N and $\tilde{\beta}_N$ in Eq. (20) are obtained by requiring the best fit of the numerical data with the theoretical curve [58]. In particular, from the values of α_N , collected in Tab. 1, one can extrapolate a prediction for the coefficient $[\Gamma(0)]^3$ in Eq. (2) at arbitrary Δ . The comparison with Eq. (5) at $\Delta = 0$ provides an independent consistency check of the whole numerical analysis, as we now discuss. In analogy with the case $\Delta = 0$, we expect that the coefficient α_N in Eq. (7) should have the following asymptotics for large N

$$\frac{\alpha_N}{N} \xrightarrow{N \gg 1} [\Gamma(0)]^3 + bN^{-2/3} + o(N^{-2/3}). \quad (21)$$

The exponent $2/3$ of the subleading term in Eq. (21) is suggested by an analogous finite-size scaling of the distribution variance discussed in [34] in the context of the quantum XXZ spin chain. Albeit the numerical methods (Ref. [34] employed DMRG techniques) and the system are different, the convergence patterns are resemblant.

A linear fit of the numerical data for α_N/N given in Tab. 1 against $N^{-2/3}$ is shown on the right panel of Fig. 6 by taking into account points at $N = 64, 128, 256$. The numerical estimate for the coefficient $[\Gamma(0)]^3$ in Eq. (2) corresponds then to y -intercept of the regression lines. The red dashed line in Fig. 6 is the exact value at $\Delta = 0$, calculated from Eq. (5) at $\eta = 0$, i.e. $[\Gamma(0)]^3 = \frac{1}{16^{2/3}} = 0.02209\dots$. The fit estimate is then in perfect agreement with such a result and confirms the validity of our approach.

5 Conclusions

In this paper, we analyzed numerically, with Monte Carlo techniques, the fluctuations of the extremal lattice path in the six vertex model with DWBC for values of the anisotropy parameter in the domain $0 \leq \Delta < 1$. Exact results at the free fermion point ($\Delta = 0$) show that the intersection of the furthest lattice path with the lattice diagonal follows the Tracy-Widom distribution. The same is true along any line parallel to the diagonal, as long as the contact point [52] of the arctic curve with the lattice is avoided. Our numerical simulations were tested thoroughly

against these analytic results, showing very good agreement already for lattices with side-length $N = 256$ and without fitting parameters.

Further, we provided strong numerical evidence that the fluctuations of the extremal lattice path follow the Tracy-Widom distribution also for values of the anisotropy parameter in the domain $0 \leq \Delta < 1$. In particular, we verified that the width of the fluctuations about the arctic curve is of order $O(N^{1/3})$ with a prefactor that could be extrapolated from the Monte Carlo data and agrees perfectly with the exact value at $\Delta = 0$.

The study presented in this paper is based on the Ansatz that also for $\Delta \neq 0$ the distributions of the extremal path intersections with any line parallel to the lattice diagonal are the same, apart from their mean and variance. The averaged distribution converges faster to the Tracy-Widom distribution. Our numerical analysis requires relatively small lattices and samples of $O(10^6)$. Therefore it is computationally less demanding than other Monte Carlo attempts to uncover the Tracy-Widom distribution [42]. The results are fully consistent with those that Ref. [34] obtained in quantum spin chains through DMRG simulations.

Our conclusions should extend also to cases $-1 < \Delta \leq 0$, which we did not analyze in this paper but belong to the same disordered phase [18] of the model. Finally, it would be interesting to study fluctuations of the boundary of the inner phase separation curve in the antiferromagnetic regime, see for instance [59] or understand the statistics of interior lattice paths [60]. To circumvent the problem of exponentially slow mixing of the Markov chain Monte Carlo dynamics for large and negative Δ , one might implement the algorithm proposed recently in [61].

Acknowledgments

We thank Alexander Abanov, Filippo Colomo, Giacomo Gori, Andrei Pronko, Herbert Spohn and Jean-Marie Stéphan for enlightening discussions and interest in this work. JV is especially grateful to Filippo Colomo and Jean-Marie Stéphan for a careful reading of the manuscript and Herbert Spohn for sharing his unpublished draft on the subject.

References

- [1] W. Feller, An Introduction to Probability Theory and Its Applications vol. I, 3rd Edition, Wiley (1991), ISBN: 978-0-471-25708-0.
- [2] A. Okunkov, Limit shapes, real and imaginary, AMS colloquium 2007, available at <http://math.columbia.edu/~okounkov/AMScolloq.pdf>.
- [3] F. Colomo and A. Sportiello, Arctic curves in the six-vertex model on generic domains: The Tangent Method, J. Phys. A 164 (2016) 1488, <https://arxiv.org/abs/1605.01388>.
- [4] R. Kenyon and A. Okounkov, Limit shapes and the complex Burgers equation, Acta Math. 199 (2007), 263–302, <https://arxiv.org/abs/math-ph/0507007>.
- [5] W. Jockusch, J. Propp, and P. Shor, Random domino tilings and the arctic circle theorem, arXiv: math.CO/9801068, <https://arxiv.org/abs/math/9801068>.
- [6] P. Ferrari and H. Spohn, Domino Tilings and the six-vertex model at its free fermion point, J. Phys. A: Math. Gen. 39 (2006), 10297-10306, <https://arxiv.org/abs/cond-mat/0605406>.

- [7] L. Pauling, The Structure and Entropy of Ice and of Other Crystals with some Randomness of Atomic Arrangement, J. Am. Chem. Soc. 57 (12): 2680-2684, (1935).
- [8] E. Lieb, Phys. Rev. 162, 162, (1967); E.H. Lieb, Phys. Rev. Lett. 18 (1967) 692; Phys. Rev. Lett. 18 (1967) 1046; Phys. Rev. Lett. 19 (1967) 108.
- [9] R.J. Baxter, Exactly solved models in statistical mechanics, Dover Book on Physics, (2008), ISBN: 978-0486462714.
- [10] V. Korepin, N. Bogoliubov and A. Izergin, Quantum inverse scattering method and correlation functions, Cambridge University Press (1993).
- [11] N. Reshetikhin, Lectures on integrable models in statistical mechanics, In: “Exact methods in low-dimensional statistical physics and quantum computing”, Proceedings of Les Houches School in Theoretical Physics, Oxford University Press, (2010), <https://arxiv.org/abs/1010.5031>.
- [12] V. Korepin, Calculation of Norms of Bethe Wavefunctions, Comm. Math. Phys. 86, 391-418 (1982).
- [13] A. Izergin, Partition Function of the 6-Vertex Model in a Finite Volume, (Russian) Dokl. Akad. Nauk USRR, v. 297, 331-333, (1987).
- [14] A. Izergin, D. Coker, and V. Korepin, Determinant formula for the six-vertex model, J. Phys. A 25 (1992), 4315–4334.
- [15] P. Zinn-Justin, Six-vertex model with domain wall boundary conditions and one-matrix model, Phys. Rev. E 62 (2000), 3411–3418, <https://arxiv.org/abs/math-ph/0005008>.
- [16] K. Eloranta. Diamond Ice. Journal of Statistical Physics 96 (1999), 1091-1109.
- [17] V. Korepin and P. Zinn-Justin. Thermodynamic limit of the six-vertex model with domain wall boundary conditions. J. Phys. A 33 (2000), p. 7053-7066, <https://arxiv.org/abs/cond-mat/0004250>
- [18] P. Bleher and K. Liechty. Random Matrices and the Six-Vertex Model. CRM Monograph Series Volume: 32, (2014), ISBN: 978-1-4704-0961-6.
- [19] F. Colomo and A. Pronko, The arctic curve in the six vertex model, J. Stat. Phys. 138, 662-700 (2010), <https://arxiv.org/abs/0907.1264>.
- [20] F. Colomo, A. Pronko and P. Zinn Justin, The arctic curve of the domain wall six vertex model in its anitferroelectric regime, J. Stat. Mech: Theor. Exp. (2010) L03002, <https://arxiv.org/abs/1001.2189>.
- [21] K. Johansson, Shape Fluctuations and Random Matrices, Commun.Math.Phys. 209, 437 - 476 (2000), <https://arxiv.org/abs/math/9903134>.
- [22] K. Johansson, The arctic circle boundary and the Airy process. The Annals of Probability (2005), Vol. 33, No. 1, p. 1-30, <https://arxiv.org/abs/math/0306216>.
- [23] H. Widom and C. Tracy, Level Spacing distributions and the Airy kernel, Commun. Math. Phys. 159 (1994) 151-174, <https://arxiv.org/abs/hep-th/9211141>.

- [24] N. Allegra, J. Dubail, J-M. Stéphan, and J. Viti. Inhomogeneous field theory inside the arctic circle. *J. Stat. Mech.* (2016) 053108, <https://arxiv.org/abs/1512.02872>
- [25] J. Baik, P. Deift and K. Johansson, On the Distribution of the Length of the Longest Increasing Subsequence of Random Permutations, *J. Amer. Math. Soc.* 12 (1999), no. 4, 1119–1178, <https://arxiv.org/abs/math/9810105>.
- [26] M. Praehofer and H. Spohn, Scale Invariance of the PNG Droplet and the Airy Process, *J. Stat. Phys.* 108 (5-6): 1071-1106 (2002), <https://arxiv.org/abs/math/0105240>.
- [27] C.Tracy and H. Widom, Asymptotics in asep with step initial condition, *Communications in Mathematical Physics* 290(1), 129 (2009), <https://arxiv.org/abs/0807.1713>.
- [28] Z. Chen, J. de Gier, I. Hiki and T. Sasamoto, Exact confirmation of 1D nonlinear fluctuating hydrodynamics for a two-species exclusion process, *Phys. Rev. Lett.* 120, 240601 (2018), <https://arxiv.org/abs/1803.06829>.
- [29] T. Sasamoto and H. Spohn, The one-dimensional KPZ equation: an exact solution and its universality, *Phys. Rev. Lett.* 104, 230602 (2010), <https://arxiv.org/abs/1002.1883>.
- [30] V. Eisler and Z. Racz, Full counting statistics in a propagating quantum front and random matrix spectra, *Phys. Rev. Lett.* 110, 060602 (2013), <https://arxiv.org/abs/1211.2321>
- [31] J. Viti, J-M. Stéphan, J. Dubail and M. Haque, Inhomogeneous quenches in a fermionic chain: exact results, *EPL* 115 (2016) 40011, <https://doi.org/10.1209/0295-5075/115/40011>.
- [32] H. Spohn, Exact solutions for kpz-type growth processes, random matrices, and equilibrium shapes of crystals, *Physica A: Statistical Mechanics and its Applications* 369(1), 71 (2006), <https://arxiv.org/abs/cond-mat/0512011>, *Fundamental Problems in Statistical Physics*.
- [33] P. Deift, Universality for mathematical and physical systems, *arXiv:math-ph/0603038* (2006), <https://arxiv.org/abs/math-ph/0603038>.
- [34] J-M. Stéphan, Free fermions at the edge of interacting systems, *SciPost Phys.* 6, 057 (2019), <https://arxiv.org/abs/1901.02770>.
- [35] J-M. Stéphan, Extreme boundary conditions and random tilings, *SciPost Phys. Lect. Notes* 26 (2021), <https://arxiv.org/abs/2003.06339>.
- [36] D. Allison and N. Reshetikhin. Numerical study of the 6-vertex model with domain wall boundary conditions. *Annales de l’Institut Fourier*, Tome 55, n° 6 (2005), p. 1847-1869, <https://arxiv.org/abs/cond-mat/0502314>.
- [37] I. Lyberg, V. Korepin, and J. Viti, The density profile of the six vertex model with domain wall boundary conditions, *J. Stat. Mech.* (2017) 053103, <https://arxiv.org/abs/1612.06758>.

- [38] I. Lyberg, V. Korepin, G. A. P. Ribeiro and J. Viti, Phase separation in the six-vertex model with a variety of boundary conditions, *J. Math. Phys.* 59, 053301 (2018), <https://arxiv.org/abs/1711.07905>.
- [39] D. Randall and P. Tetali. Analyzing Glauber dynamics by comparison of Markov chains. *Journal of Mathematical Physics*, 41(3):1598–1615, 2000, <https://doi.org/10.1063/1.533199>.
- [40] T. Liu, Torpid mixing of Markov chains for the six-vertex model on \mathbb{Z}_2 . In *Approximation, Randomization, and Combinatorial Optimization. Algorithms and Techniques (APPROX/RANDOM 2018)*, <https://arxiv.org/abs/1809.02703>.
- [41] M. Fahrback and D. Randall, Slow Mixing of Glauber Dynamics for the Six-Vertex Model in the Ordered Phases, *Proceedings of the 23rd International Conference on Randomization and Computation (RANDOM 2019)*, <https://arxiv.org/abs/1904.01495>.
- [42] C. Mendl and H. Spohn, Searching for the Tracy-Widom distribution in nonequilibrium processes, : *Phys. Rev. E* 93, 060101(R) (2016) <https://arxiv.org/abs/1512.06292>.
- [43] K. Eloranta, The bounded 19-vertex model (2017) <https://arxiv.org/abs/1710.03609>; K. Eloranta, The bounded 15-vertex model (2018), <https://arxiv.org/abs/1807.07567>.
- [44] R. Keesman and J. Lamers, A numerical study of the F-model with domain-wall boundaries, *Phys. Rev. E* 95, 052117 (2017), <https://arxiv.org/abs/1702.05474>.
- [45] D. Keating and A. Sridhar, Random Domino Tilings with the GPU, *J. Math. Phys.* 59, 091420 (2018), <https://arxiv.org/abs/1804.07250>.
- [46] B. Debin, P. Di Francesco and E. Guitter, Arctic curves of the twenty-vertex model with domain wall boundaries, *J Stat Phys* 179, 33-89 (2020), <https://arxiv.org/abs/1910.06833>.
- [47] J-F. de Kemmeter, B. Debin and P. Ruelle, Arctic curves of the 6V model with partial DWBC and double Aztec rectangles, *J. Phys. A: Math. Theor.* 55 (2022) 305004, <https://arxiv.org/abs/2203.08506>.
- [48] P. Belov and N. Reshetikhin, The two-point correlation function in the six-vertex model, *J. Phys. A: Math. Theor.* 55 155001 (2022), <https://arxiv.org/abs/2012.05182>.
- [49] G. T. Barkema and M. E. J. Newman. Monte Carlo simulation of ice models. *Phys. Rev. E* 57 (1998), 1155, <https://arxiv.org/abs/cond-mat/9706190>.
- [50] O. F. Syljuåsen and M. B. Zvonarev. Directed-loop Monte Carlo simulations of vertex models. *Phys. Rev. E* 70 (2004), 016118, <https://arxiv.org/abs/cond-mat/0401491>.
- [51] F. Alet, Y. Ikhlef, J. Jacobsen, G. Misguich and V. Pasquier, Classical dimers with aligning interactions on the square lattice, *Phys. Rev. E* 74, 041124 (2006), <https://arxiv.org/abs/cond-mat/0607747>.

- [52] V. Gorin, From Alternating Sign Matrices to the Gaussian Unitary Ensemble, *Comm. Math. Phys.*, 332, no. 1 (2014), <https://arxiv.org/abs/1306.6347>.
- [53] V. Kapitonov and A. Pronko, Six-Vertex Model as a Grassmann Integral, One-Point Function, and the Arctic Ellipse, *Journal of Mathematical Sciences* volume 264, pages 313–346 (2022), <https://doi.org/10.1007/s10958-022-06000-w>
- [54] M. Hollander, D. Wolfe and E. Chicken, *Nonparametric Statistical Methods*, John Wiley and Sons, 3rd Edition, 2015.
- [55] A. N. Kolmogorov, Sulla determinazione empirica di una legge di distribuzione. *Giorn. Ist. Ital. Attuari* 4, 83-91 (1933).
- [56] W. Feller, On the Kolmogorov-Smirnov Limit Theorems for Empirical Distributions. *Annals of Mathematical Statistics*, 19, 177-189 (1948) <https://doi.org/10.1214/aoms/1177730243>
- [57] J. Vrbik, Deriving CDF of Kolmogorov-Smirnov Test Statistic. *Applied Mathematics*, 11, 227-246 (2020) <https://doi.org/10.4236/am.2020.113018>.
- [58] <https://reference.wolfram.com/language/ref/FindFit.html>
- [59] S. Chhita and K. Johansson, Domino statistics of the two-periodic Aztec diamond, *Advances in Mathematics* 294 (2016) 37–149, <https://arxiv.org/abs/1410.2385>
- [60] B. Debin, J-F. de Kemmeter and P. Ruelle, Fluctuations and arctic curve in the Aztec diamond, <https://arxiv.org/abs/2301.00600>
- [61] J-Y. Cai and T. Liu, An FPTAS for the square lattice six-vertex and eight-vertex models at low temperatures, *Proceedings of the 2021 ACM-SIAM Symposium on Discrete Algorithms SODA* (2021), <https://epubs.siam.org/doi/abs/10.1137/1.9781611976465.92>